Engineering Structures 309 (2024) 118050

Contents lists available at ScienceDirect

Engineering Structures

journal homepage: www.elsevier.com/locate/engstruct

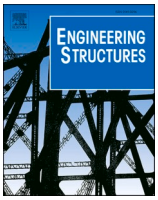

Effect of sustained loads on the durability of GFRP bars with and without UHP-ECC cover

Zhi-Hao Hao [a], Jun-Jie Zeng [b,*]

[a] Department of Civil and Environmental Engineering, The Hong Kong Polytechnic University, Hong Kong, China
[b] UniSA STEM, University of South Australia, South Australia 5095, Australia

ARTICLE INFO

Keywords:
GFRP bar
Engineered cementitious composites (ECC)
Ultra-high-performance concrete (UHPC)
Durability
Sustained load

ABSTRACT

Fiber-reinforced polymer (FRP) bar reinforced ultra high-performance engineered cementitious composite (UHP-ECC) structures (referred to as FRP-UHP-ECC structures) have been demonstrated to have excellent mechanical properties, while their durability in the alkaline environment has never been explored, particularly when being subjected to tensile loadings. To this end, this article aims to investigate the effects of sustained loads on the durability performance of Glass FRP (GFRP) bars embedded in UHP-ECCs while immersed in an alkaline solution. The test results revealed that the effect of elevated temperatures was exacerbated when specimens were subjected to even a low sustained load (20 % of ultimate strength). Furthermore, UHP-ECC covers considerably postponed the degradation of GFRP bars. Nevertheless, the protective effects of UHP-ECC covers were nearly entirely compromised when the specimens were subjected to sustained loads. The findings of this study provide useful knowledge for a comprehensive evaluation of the durability of GFRP bars under UHP-ECC environments.

1. Introduction

The social and economic development of coastal cities is greatly dependent on marine infrastructure [1–5]. These structures face challenges arising from both mechanical and environmental aspects [6,7]. To this end, a novel composite structure, fiber-reinforced polymer (FRP) bars reinforced ultra high-performance engineered cementitious composite (UHP-ECC) known as FRP-UHP-ECC structures, has been proposed [8–10]. FRP-UHP-ECCs have excellent mechanical properties, characterized by their tensile strain-hardening, multiple-cracking abilities, and ultra high compressive strength [11–17], which make them well-suited to meet the demanding mechanical requirements in marine environments. The synergies between these materials can effectively address specific limitations inherent to each material. The relatively weak stiffness of FRP reinforced normal concrete structures, attributed to the low elastic modulus of FRP, can be well addressed by using FRP-UHP-ECCs owing to the larger elastic modulus of UHP-ECC compared to that of normal concrete. The remarkable ductility of ECC can mitigate the inherent elastic brittleness associated with FRP bars [18]. Incorporating FRP bars in UHP-ECCs can decrease the reliance on short fibers to achieve a desirable tensile strain-hardening behavior [8–10]. Furthermore, the absence of traditional steel reinforcements, replaced by FRP reinforcement with excellent corrosion resistance [19–25], enhances the durability of FRP-UHP-ECCs. This corrosion resistance is crucial for withstanding the aggressive marine environment, thus reducing the costs of maintenance and repair.

Glass FRP (GFRP) bars are frequently favored in civil engineering for their cost-effectiveness and favorable mechanical performance [26,27]. Despite being non-metallic, GFRP bars still exhibit degradation in alkaline concrete environments [28–32]. The fundamental silicon-oxygen structures, comprising approximately 55 % of the glass fiber, are susceptible to alkalis due to chemical reactions (i.e., etching and leaching). These reactions impact the glass fiber, leading to tensile strength decreases [33,34]. While the resin offers protection to glass fibers, alkalis and moisture can still permeate the bars. Furthermore, the matrix undergoes plasticization and hydrolysis when exposed to moisture [32,35].

To assess the long-term performance of GFRP bars, extensive accelerated tests have been conducted [36–40]. The findings reveal that higher temperatures, larger pH and prolonged exposure durations are associated with more pronounced degradation of GFRP bars [41,42]. Furthermore, several studies highlighted a significant degradation of FRP bars when directly exposed to alkaline solutions compared to embedded within concrete. [43–45]. Upon direct immersion of bare FRP

* Corresponding author.
E-mail addresses: zhihao.hao@connect.polyu.hk (Z.-H. Hao), jun-jie.zeng@unisa.edu.au (J.-J. Zeng).

https://doi.org/10.1016/j.engstruct.2024.118050
Received 30 December 2023; Received in revised form 3 March 2024; Accepted 10 April 2024
Available online 22 April 2024

bars in alkaline solutions, degradation uniformly occurs across their entire surface, facilitated by unrestricted movement of moisture and alkalis around the bars. Conversely, the concrete cover impedes the diffusion of moisture and alkalis, posing a greater challenge for their further diffusion. Moreover, the interaction between FRP bars and the pore solution is confined to a limited area due to the presence of aggregates. For the FRP-UHP-ECC structure, the UHP-ECC cover demonstrates lower water permeability in comparison to ordinary concrete, which is anticipated to provide better protection for GFRP bars.

The effect of sustained loads on the durability of FRP has been investigated, which represents the actual operational conditions [28,34,46–48]. When subjected to sustained loads, the defects in FRP can expand, accelerating the diffusion of moisture and alkalis, and consequently accelerating the degradation process. Some studies found that low-stress levels (e.g., ≤20 % of ultimate strength) minimally accelerated the degradation, whereas high-stress levels (e.g., ≥20 %) had a pronounced accelerating effect on degradation [28,46,47].

To this end, this study is designed to investigate the effects of sustained loads and UHP-ECC covers on the durability of GFPP bars. GFRP bars were wrapped within UHP-ECC covers and immersed in an alkaline solution while being subjected to sustained loads. The tensile properties of GFRP bars before and after exposure were tested to evaluate their durability. Scanning electron microscopy (SEM) and X-ray computed tomography (CT) tests were performed to further explore the mechanisms of their degradation.

2. Experiment grogram

2.1. GFRP bar

GFRP bars used in this study were fabricated by Dextra Building Materials (Guangdong) Co., Ltd. They were manufactured through the pultrusion process with a nominal diameter of 10 mm and a fiber volume content of 81.2 %. The glass transition temperature of the GFRP bar is approximately 110 ℃. The surface of GFRP bars was helically wrapped with a polyethylene fiber bundle and coated with a thin layer of fine sand to enhance the bond performance, as shown in Fig. 1.

2.2. UHP-ECCs

UHP-ECCs used in this study comprised Ordinary Portland cement (P.II.52.5 R), silica sand with particle sizes ranging from 0.076 mm to 0.150 mm, silica fume with particle sizes ranging from 0.1 μm to 1 μm, and ground granulated blast furnace slag (GGBFS). The water-to-binder ratio was 0.127. The polyethylene (PE) fibers used in this study possess dimensions of 18 mm in length and 24 μm in diameter, and a density of 0.97 g/cm^3. Their tensile strength and modulus are 3.0 GPa and 116 GPa, respectively. The volume ratio of PE fiber is 1.96 %. The detailed compositions of UHP-ECCs are listed in Table 1.

The compressive properties of UHP-ECCs were evaluated by 100 mm (height) × 50 mm (diameter) cylindrical specimens. The compressive strength and modulus were 119.2 MPa and 37.9 GPa, respectively, with an ultimate strain (i.e., the strain corresponding to the ultimate compressive strength) of 3337 $\mu\varepsilon$ and a Poisson's ratio of 0.26. The tensile properties of UHP-ECCs were assessed using dumbbell-shaped samples (Fig. 2) following JSCE's recommendation [49]. The tensile stress-strain responses demonstrated strain-hardening characteristics (Fig. 3). The ultimate tensile strength and ultimate strain were determined to be 9.13 MPa and 3.68 %, respectively.

Table 1
Mix proportions of UHP-ECC.

Raw material	Amount
Cement (C) (kg/m^3)	800
Silica sand (kg/m^3)	500
Silica fume (SF) (kg/m^3)	150
Ground granulated blast furnace slag (GGBFS) (kg/m^3)	750
Water (W) (kg/m^3)	260
Polyethylene (PE) fiber (kg/m^3)	19
Superplasticizer (kg/m^3)	40
W/(C+SF+GGBFS)	0.127

2.3. Specimens and exposure conditions

Accelerated aging tests were conducted on GFRP bars with a length of 1000 mm, which were immersed in an alkaline solution with a pH value of 12.6. The compositions of the alkaline solution are provided in Table 2.

Before immersion, selected GFRP bars were wrapped in UHP-ECCs and/or subjected to sustained loads. In the case of UHP-ECC embedded specimens, GFRP bars were centrally embedded in UHP-ECCs with a 50 mm diameter. Epoxy was used to seal both ends of UHP-ECC covers to prevent longitudinal diffusion. The sustained load was applied using a container equipped with a built-in thermostatic device designed by Zeng et al. [26], as shown in Fig. 4. This apparatus employs a unique lever mechanism, deviating from conventional hydraulic jacks or springs, to effectively counteract load loss arising from variations in the mechanical properties of the bars. Consequently, it obviates the necessity for load adjustments to maintain a consistent load. Prior to the application of sustained loads, both ends of GFRP bars were

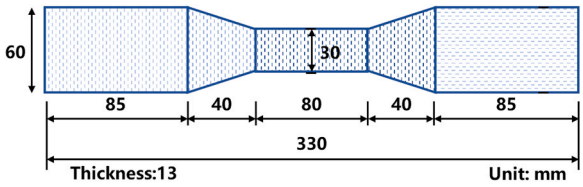

Fig. 2. Specimen for direct tension test.

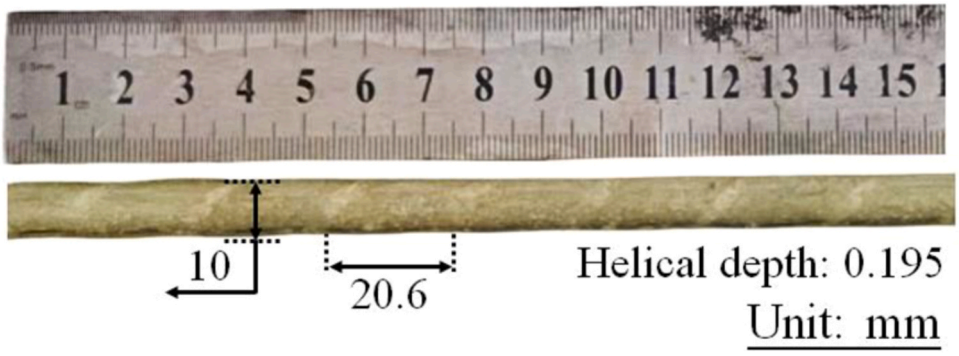

Fig. 1. GFRP bars.

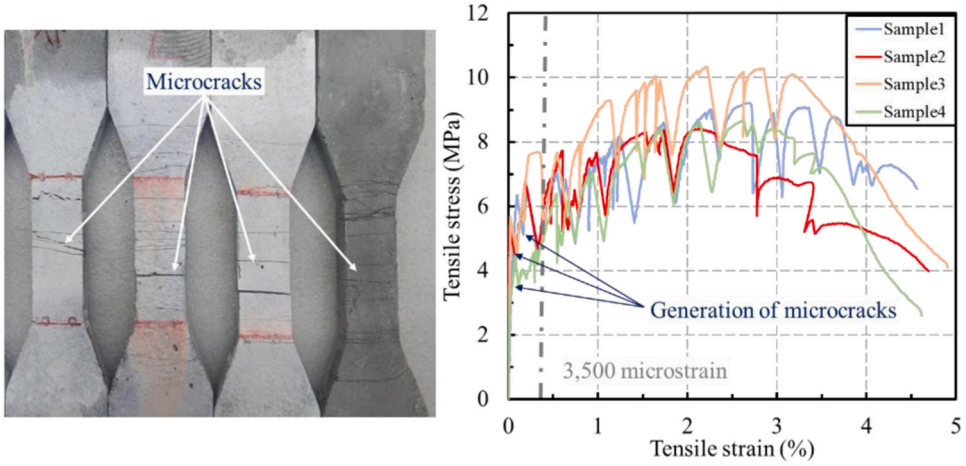

Fig. 3. Tensile behavior of dumbbell-shaped UHP-ECCs.

Table 2
Chemical compositions of alkaline solution.

$Ca(OH)_2$	NaOH	KOH	pH
118.5 g/liter	0.9 g/liter	4.2 g/liter	12.6

secured with steel tubes with 300 mm in length. Sika 330 epoxy was utilized to fill the gap between the GFRP bar and the steel tube. Plastic caps, featuring a central opening for bars, sealed both ends of each steel anchorage tube to prevent epoxy leakage. During the epoxy curing process, the specimens were affixed to an L-shaped steel bar to ensure alignment. Following 7-day epoxy curing, one end of the GFRP bar was positioned against the outer surface of the container, while the other end was connected to the lever device. During immersion, silicone waterproof glue sealed the gaps. The lever device comprises two steel levers connected in series, with each lever providing a load amplification factor of 10, leading to a total factor of 100. The constant sustained tensile load was applied to GFRP bars by suspending designed-weight blocks. In the present study, the specifically designed sustained load generated a strain of 3500 microstrains in the GFRP bars [50], which aligned with a stress level approximately equivalent to 20 % of their tensile strength.

In addition, 40 ℃ was used to accelerate degradation, which is a common temperature in accelerated aging tests [30,43]. Several studies have highlighted that temperatures exceeding 60 ℃ might trigger unforeseen physical or chemical changes in GFRP bars, making them an inadequate representation of the actual deterioration process [26].

The test program is outlined in Table 3. For ease of identification, each specimen is labeled with a name starting with a letter denoting exposure temperature ("TR" and "T40″ for room temperature and 40 ℃), followed by "S0″ or "S20″ to indicate with or without sustained load (i.e., 20 %); and "C" or "U" to distinguish with or without UHP-ECC covers; The notation "D* " specifies the immersion duration, with "* " signifying exposure days. Each testing condition utilized four replicate specimens.

2.4. Test methods

2.4.1. Tension test

Following exposure, the UHP-ECC cover was carefully removed avoiding any damage to GFRP bars. Both ends of the bars were anchored within steel tubes (300 mm in length), and filled with Sika 330 epoxy. The specially designed steel frame (Fig. 5) was used for the tensile test. Tensile loads were applied using a hydraulic jack at a stress rate of 250 MPa/min [51], and an extensometer was employed to record the elongation of GFRP bars. The tensile modulus was calculated as the secant modulus, defined as the slope between approximately 25 % and 50 % of the ultimate load according to CSA-S806 [51].

Table 3
Test programs.

Specimens ID	Temperature (℃)	Sustained load	Concrete cover	Duration (days)
TR-S0-C-D*	Room temperature	×	√	0, 90, 180, 270, 360
TR-S20-C-D*		√	√	0, 90, 180
T40-S0-U-D*	40	×	×	0, 90, 180
T40-S0-C-D*		×	√	0, 90, 180, 270, 360
T40-S20-C-D*		√	√	0, 90, 180

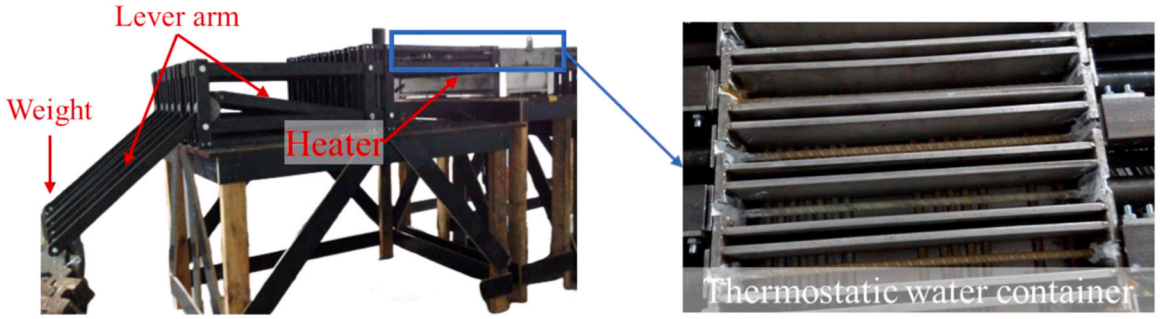

Fig. 4. The lever device [26].

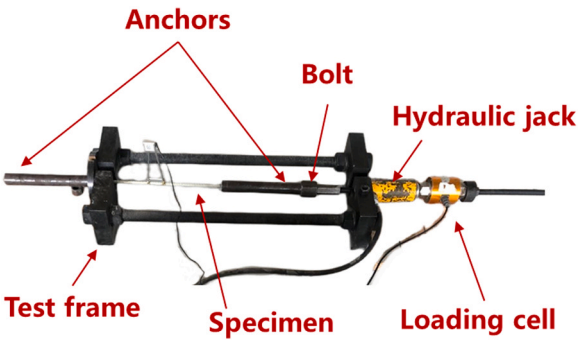

Fig. 5. Setup for the tensile test.

2.4.2. X-ray computed tomography (CT)

In recent years, X-ray computed tomography (CT) scanning technology has emerged as a valuable diagnostic tool for assessing the microstructure of FRP [52]. Offering non-destructive capabilities, 3D imaging and high resolution, X-ray CT is frequently employed to examine fibers and defects in FRP composites [31,53,54].

In the present study, the 3D structures of GFRP bars were observed by an ultra-high resolution NanoVoxel 3000D. Scans were conducted on small segments of GFRP bars, approximately 1 cm in length. The scans were executed with a 100 kV source voltage, a 5 W power and voxel sizes ranging from 10–15 μm. The projection images were reconstructed using Avizo2019.1 software, and the image segmentation was manually performed using the histogram. Employing image analysis, the distribution and volume content of various components, including fiber, resin, and void, within the GFRP bars were quantified.

2.4.3. Scanning electron microscope (SEM)

To examine the morphologies of the cross-section of GFRP bars, the scanning electron microscope (SEM) was conducted by a TM3030 SEM machine. Prior to testing, GFRP bars underwent a coating process with an extremely thin layer of gold film in a vacuum to enhance their electrical conductivity. The electron acceleration voltage was set as 10 kV. For cross-section morphology observation, GFRP bars were cut and embedded in epoxy, and their cross-sections were subsequently ground and polished.

3. Results and discussions

The GFRP bars displayed an almost linear behavior until reaching failure, characterized by fiber rupture and accompanied by fiber and resin delamination. The failure modes of these bars remained consistent before and after exposure.

Table 4 shows the changes in tensile properties of GFRP bars before and after exposure, with a coefficient of variation (COV) within 5 %, indicating minimal variations. The observed reductions in tensile strength are attributed to both moisture diffusion and alkaline attacks. The polymer matrix experiences disruption in intermolecular forces and weakening of polymer chains due to moisture absorption, a phenomenon known as plasticization. Additionally, the alkali, which infiltrates with moisture, chemically degrades both the fibers and the matrix [26].

Fig. 6 presents a comparison of the tensile elastic moduli of GFRP bars under different conditions, revealing minor fluctuations as exposure time increases. The results indicate that the elastic moduli were not significantly affected after exposure, with retentions exceeding 90% even after 180 days. Notably, bars without UHP-ECC covers (i.e., T40-S0-U) exhibited a continuous decrease in elastic moduli but still retained 90.2% after 180 days.

While degradation may manifest in the matrix and fiber-to-matrix interface as a result of environmental exposure, the fibers themselves may show minimal impact, especially with relatively limited exposure time. It can be attributed to the protective role of the matrix, which can be confirmed through SEM analysis, as discussed in the following section. As a consequence, the stress-strain curves under low loads remained relatively similar for the GFRP bars before and after exposure, resulting in limited effects on the modulus of elasticity.

Table 4
Tensile properties of GFRP bars before and after exposure.

Specimens ID	Tensile strength			Modulus of elasticity		
	Mean (MPa)	Retention (%)	COV (%)	Mean (GPa)	Retention (%)	COV (%)
TR-S0-C-D0	1129.6	100.0	1.6	48.6	100.0	1.1
TR-S0-C-D90	1062.0	94.0	1.0	50.6	104.1	1.3
TR-S0-C-D180	1004.6	88.9	3.4	51.9	106.8	3.2
TR-S0-C-D270	994.7	88.1	1.1	48.2	99.3	2.2
TR-S0-C-D360	963.5	85.3	1.8	50.7	104.3	2.8
TR-S20-C-D90	932.4	82.5	3.3	47.6	98.0	2.1
TR-S20-C-D180	905.5	80.2	2.2	48.7	100.4	1.0
T40-S0-U-D90	869.3	77.0	2.6	44.4	91.4	4.0
T40-S0-U-D180	724.4	64.1	1.0	43.8	90.2	4.2
T40-S0-C-D90	1014.8	89.8	1.2	48.7	100.3	4.3
T40-S0-C-D180	986.3	87.3	3.1	51.1	105.2	3.4
T40-S0-C-D270	925.0	81.9	2.4	47.0	96.7	1.5
T40-S0-C-D360	912.6	80.8	3.5	47.5	97.9	1.9
T40-S20-C-D90	828.7	73.4	3.0	51.9	106.8	1.5
T40-S20-C-D180	762.8	67.5	2.1	46.9	96.6	2.2

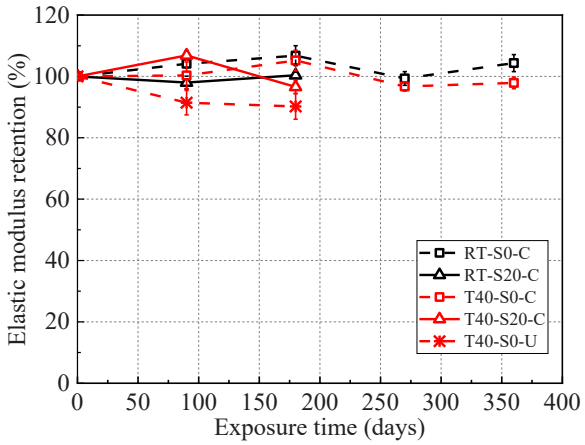

Fig. 6. Changes in elastic modulus of GFRP bars over time.

3.1. Effect of temperatures

As shown in Fig. 7, GFRP bars under a higher temperature of 40 ℃ show more pronounced reductions in tensile strength. Specifically, compared to UHP-ECC embedded bars at room temperature without loads (i.e., TR-S0-C), those at 40 ℃ (i.e., T40-S0-C) exhibited 4.2 % and 1.6 % greater reductions in tensile strength after 90 and 180 days, respectively. In comparison, the GFRP bars subjected to sustained loads at 40 ℃ (i.e., T40-S20-C) showed 9.2 % and 12.6 % more reductions in tensile strength, compared to those with sustained loads at room

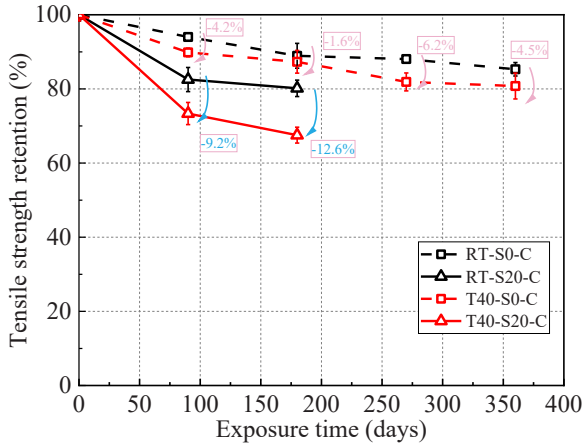

Fig. 7. Effect of temperatures on the tensile strength retentions of GFRP bars.

temperature (i.e., TR-S20-C). This suggests that elevated temperatures exert a more significant accelerating effect on GFRP bars subjected to sustained loads.

Undoubtedly, temperatures have been shown to accelerate the degradation of GFRP bars, as demonstrated in various studies [31,41,55]. This phenomenon is attributed to the heightened mobility of moisture and alkalis at elevated temperatures, thereby expediting the degradation process. Furthermore, sustained loads induce microcracks in both the UHP-ECCs and GFRP bars. These microcracks serve as conduits for moisture and alkalis, intensifying the degradation process, which can be further accelerated by elevated temperature. This study revealed an exacerbation of the accelerated effect, even when specimens were subjected to low sustained loads (20 % of ultimate strength). Previous studies predominantly focused on either temperatures or sustained loads individually. This highlights the importance of future accelerated tests that should consider both sustained loads and elevated temperatures, providing a more comprehensive exploration of the accelerated effects of elevated temperatures at different load levels. Such investigations are crucial for informing the long-term design considerations of structures incorporating FRP under in-service conditions.

3.2. Effect of sustained loads

Fig. 8 reveals a notably more pronounced degradation of GFRP bars with sustained loads compared to those without sustained loads. Compared to those without sustained loads (i.e., TR-S0-C and T40-S0-C), the tensile strength of stressed GFRP bars (i.e., TR-S20-C and T40-S20-C) exhibited 8.8 % and 19.8 % more reductions at room temperature and

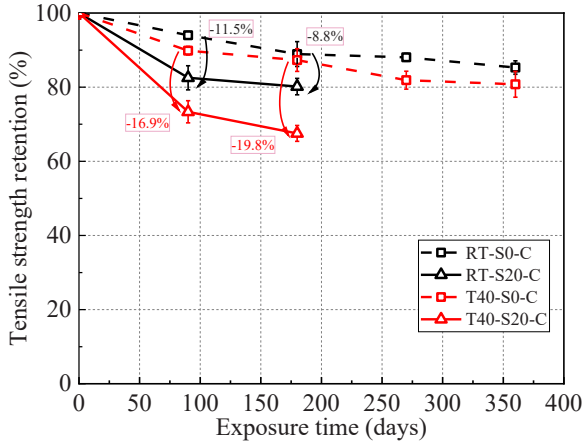

Fig. 8. Effect of sustained loads on the tensile strength retentions of GFRP bars.

40 ℃, respectively after 180 days. This also highlights the combined accelerated effects of elevated temperatures and sustained loads on the degradation of GFRP bars.

The more significant degradation observed in GFRP bars under sustained loads can be attributed to the microcracks induced by the sustained loads, as shown in Fig. 9. The sustained load leading to 3500 microstrains on GFRP bars can induce cracks in UHP-ECC covers, as evidenced by curves in Fig. 3. For GFRP bars without sustained loads, concentration gradients serve as the only mechanisms for the diffusion of moisture and alkalis into the GFRP bars, which occurs at a slower rate. Sustained loads induce microcracks in both the matrix and UHP-ECC covers, enabling a faster ingress of moisture and alkali into the interior of GFRP bars.

While some studies have reported limited effects of sustained loads on the degradation of FRP bars when the sustained loads were at lower levels (i.e., less than 20 % of ultimate strength) [28,56], the present study reveals that even when subjected to lower-level sustained loads, the UHP-ECC embedded GFRP bars exhibited more pronounced degradation compared to those without sustained loads. This distinction arises from the use of UHP-ECC embedded bars in this study, whereas previous studies exposed bare bars to the environment. Although the sustained load may exert limited effects on the degradation of GFRP bars, the induced cracks in UHP-ECC covers can result in diminishment in the protective effects of UHP-ECCs. These reductions allows more moisture and alkalis to reach the internal GFRP bars, leading to severe degradation. This highlights the importance of considering the effects of sustained loads on the degradation of FRP bars in concrete environments, rather than only focusing on bare bars, as they are under distinctly different conditions.

3.3. Effect of UHP-ECC covers

Fig. 10 reveals that UHP-ECC covers significantly delays the degradation of GFRP bars. Compared to bars without UHP-ECC covers (i.e., T40-S0-U), the UHP-ECC embedded GFRP bars (i.e., T40-S0-C) exhibited 12.9 % and 23.2 % less reductions in tensile strength after 90 and 180 days, respectively. However, when UHP-ECC embedded GFRP bars were subjected to sustained loads (i.e., T40-S20-C), the protective effects were compromised. Compared to bars without UHP-ECC covers (i.e., T40-S0-U), UHP-ECC embedded GFRP bars subjected to sustained loads (i.e., T40-S20-C) exhibited similar degradation, with 3.6 % more and 3.4 % less reductions after 90 and 180 days, respectively.

As discussed before, lower sustained loads have limited effects on the degradation of FRP bars (less than 20 % of ultimate strength) [28,56]. In addition, the degradation observed in both bare bars and UHP-ECC embedded bars with sustained loads (i.e., T40-S20-C and T40-S0-U) exhibited comparable degradation after the same exposure time. This indicates that the protective effects of UHP-ECC covers were nearly completely diminished when subjected to low sustained loads. This once again emphasizes the importance of accounting for the effects of the

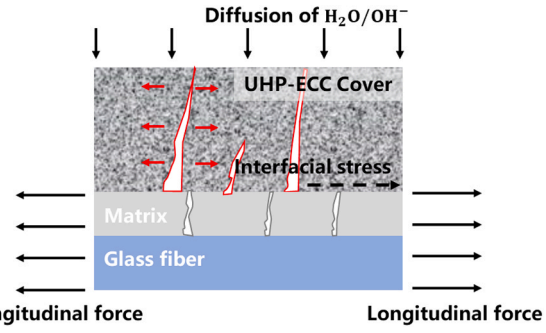

Fig. 9. Illustration of the effect of sustained loads on UHP-ECC embedded GFRP bars.

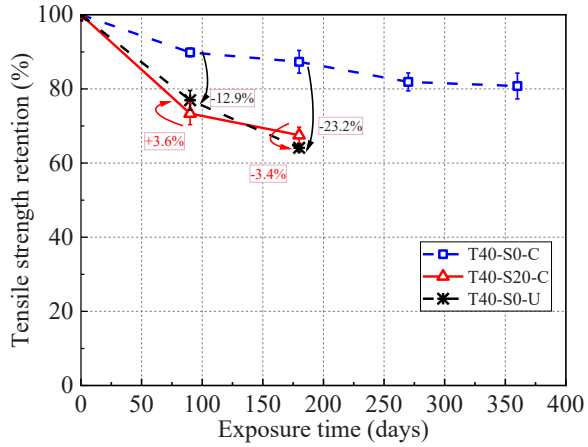

Fig. 10. Effect of UHP-ECC covers on the tensile strength retentions of GFRP bars.

sustained load on the degradation of FRP bars in concrete environments, enabling a more accurate simulation of in-service conditions.

3.4. SEM images

To explore the degradation mechanism of GFRP bars, SEM analysis was carried out on selected GFRP specimens, including those without exposure, V-S0-C-D180, V-S0-U-D180 and V-S20-C-D180, as shown in Fig. 11. In the case of GFRP bars without exposure, the cross-section is relatively intact, only with some minor voids, likely induced during the manufacturing process. Notably, the glass fibers and matrix also exhibit integrity, showcasing robust bonds at the fiber-to-matrix interface.

In the GFRP bars after exposure, visible voids emerge in their cross sections, which is primarily attributed to the hydrolysis of the matrix induced by moisture and alkalis (Eq. 1). The ester groups within the vinyl ester matrix are susceptible to hydrolysis, which can lead to the rupture of long chains and the generation of monomers. Then, it results in a reduction in matrix integrity. Furthermore, these voids are more concentrated at the edges. It suggests that the degradation occurred from the edge toward the inside of GFRP bars due to the diffusion of moisture and alkalis.

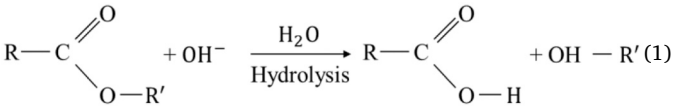

On the other hand, the glass fibers retain relative integrity, indicating minimal degradation. Based on this observation, it can be inferred that the current stage of GFRP bar degradation primarily arises from matrix degradation. This degradation hinders the efficient transfer of stress between fibers, ultimately resulting in the strength reduction of GFRP bars.

Upon closer observation, in the T40-S0-C-180 specimen, these voids are relatively small and distributed in a dotted pattern. However, in the T40-S0-U-180 and T40-S20-C-180 specimens, which exhibited comparable and more pronounced degradation, the voids in their cross-sections are relatively larger and denser. Moreover, these voids are interconnected, forming patches (i.e., connected voids). The more pronounced degradation of GFRP bars appears to be associated with the increase in porosity or connected porosity of the cross-section. Therefore, for future research, a more systematic approach to evaluating the durability of FRP materials may involve quantifying the relationship between the development of porosity (or connected porosity) due to exposure and their mechanical strength reduction. In addition, larger connected porosity was observed in the T40-S0-U-180. This observation could be attributed to a higher concentration of micro defects introduced during the manufacturing process in the specimen, making it more susceptible to connectivity due to matrix degradation.

3.5. X-ray CT results

3D X-ray CT tests were also carried out on selected GFRP specimens, including those without exposure, T40-S0-C-D90, T40-S20-C-D90 and

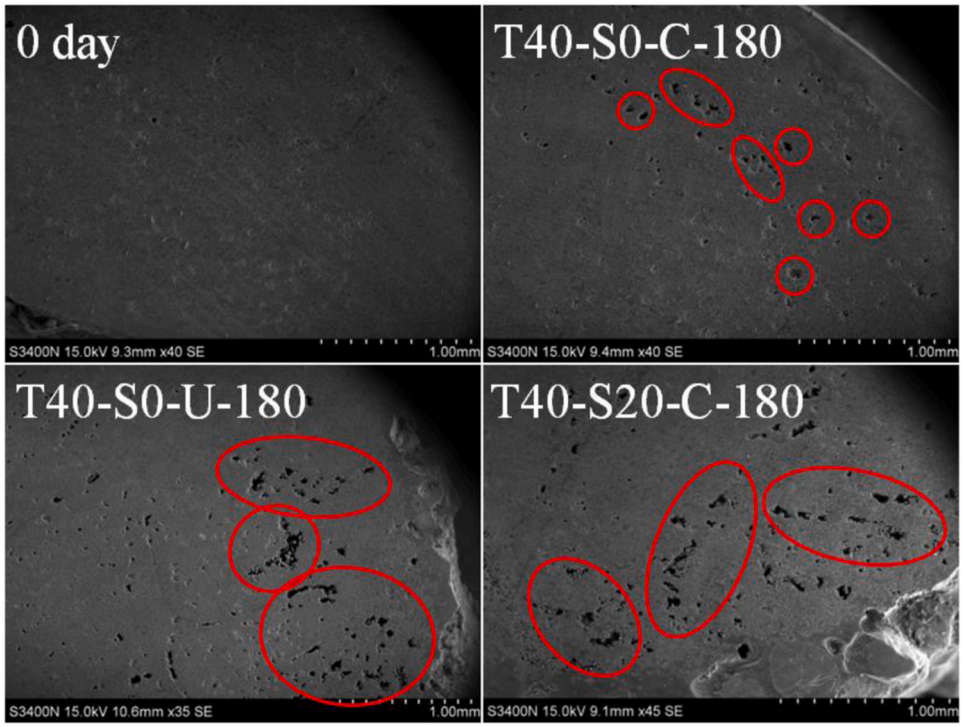

Fig. 11. SEM images for GFRP bars before and after exposure.

T40-S0-U-D90. Fig. 12 presents the 3D X-ray CT images of GFRP bars to primarily quantify the contents of each component, where two of these images (i.e., unexposed and T40-S20-C-D90) were reproduced from by Zhou et al. [57]. For the GFRP bar without exposure, regular and compact fiber distribution is observed. Its matrix is almost uniformly distributed across the cross-section. Furthermore, the GFRP bar without exposure presents minimal void, indicating effective infiltration of fibers by the matrix.

Following exposure, there are noticeable increases in the volume content of voids, aligning with SEM observations. In the T40-S0-C specimen, the void content increases to 3.2 %, while the T40-S20-C and T40-S0-U specimens increase to 6.4 % and 6.1 %, respectively. The more significant increases in void content exactly correlate with the more pronounced degradation of GFRP bars. In addition, the T40-S20-C and T40-S0-U specimens exhibited comparable reductions in tensile strength, aligning with their similar increases in void contents. These consistent patterns further confirm a relationship between the development of porosity and material degradation. Therefore, it is rational to investigate this relationship in future research for a more comprehensive evaluation of FRP durability.

In addition, there is a distinct alteration in matrix distribution after exposure. The matrix becomes concentrated in the center of the bars, while the matrix at the edges gradually reduces, which indicates outer-to-inner degradation of GFRP bars (Eq. 1). On the other hand, Fig. 12 shows that some generated voids exhibit a radial distribution, which is because that the penetration of moisture and alkalis through microcracks in GFRP bars in more rapid. Therefore, the degradation of the matrix initiated early, even in the inner part of GFRP bars, leading to the observation of larger voids in the inner region. The microcracks are more likely to originate in the area characterized by larger connected porosity. This underscores the significance of connected porosity in GFRP bars concerning their durability performance.

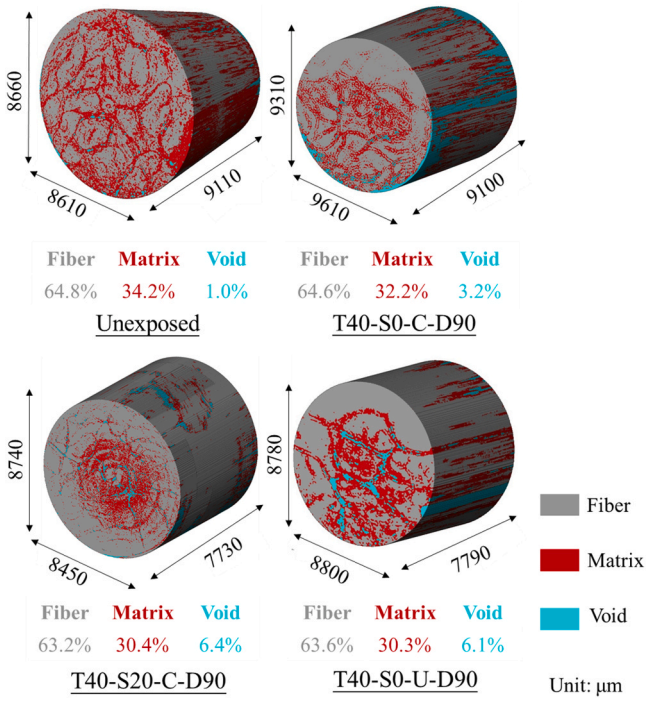

Fig. 12. X-ray CT images for GFRP bars before and after exposure (Images of unexposed and T40-S20-C-D90 were reproduced from by Zhou et al. [57]).

4. Conclusions

In this study, the effects of sustained loads on the durability performance of GFRP bars, both with and without UHP-ECC covers were investigated. The degradation mechanism was further explored based on SEM and X-ray CT analysis. Drawing insights from the test results and discussions, the following conclusions can be inferred:

1. The accelerated effect of elevated temperatures was greatly exacerbated when specimens were subjected to even a low sustained load (20 % of ultimate strength). This emphasizes the necessity of exploring the combined effects of elevated temperatures with different load levels. Such investigations are crucial for the long-term design considerations of FRP-incorporated structures under in-service conditions.
2. In contrast to previous studies, this study found that even lower-level sustained loads (i.e., 20 %) induced evidently more pronounced degradation of UHP-ECC embedded GFRP bars compared to those without sustained loads. After 180 days of exposure at 40 °C, the stressed GFRP bars exhibited a 19.8% greater reduction in strength compared to those without sustained loads. This highlights the importance of considering the effects of sustained loads on the degradation of FRP bars embedded in concrete environments, rather than only focusing on bare bars.
3. UHP-ECC covers significantly postponed the degradation of GFRP bars. After 180 days of exposure at 40 °C, the UHP-ECC embedded GFRP bars exhibited a 23.2% smaller reduction in strength compared to those without UHP-ECC covers. Nevertheless, the protective effects of UHP-ECC covers were nearly entirely compromised when the specimens were subjected to a sustained load due to microcracks in UHP-ECCs induced by sustained loads. This again highlights the importance of future research to account for the effects of sustained loads on the protection of concrete covers to more accurately simulate in-service conditions.
4. The microcharacterization (i.e., SEM and X-ray CT) of GFRP bars indicates that the more pronounced degradation may be associated with the development of porosity or connected porosity after exposure. Therefore, future research could focus on establishing the relationship between the development of porosity (or connected porosity) and their durability performance, aiming for a more comprehensive evaluation of FRP durability.
5. This study preliminarily explores the impact of UHP-ECC covers and sustained loads on the durability of GFRP bars. In addition, the rheological properties (e.g., permeability) of UHP-ECC covers are also crucial factors affecting the degradation of embedded FRP bars. Future research should investigate various types and sizes of UHP-ECC covers, as well as different levels of sustained loads, to gain a more comprehensive understanding of their influence. This broader investigation will contribute to the development of safer designs.

CRediT authorship contribution statement

Jun-Jie Zeng: Writing – review & editing, Validation, Supervision, Resources, Project administration, Funding acquisition, Data curation, Conceptualization. **Zhi-Hao Hao:** Writing – original draft, Investigation, Formal analysis, Data curation.

Declaration of Competing Interest

The authors declare that they have no known competing financial interests or personal relationships that could have appeared to influence the work reported in this paper.

Data Availability

Data will be made available on request.

Acknowledgements

The authors acknowledge the financial support received from the Australian Research Council (DE220100406).

References

[1] Qu F, Li W, Dong W, Tam VW, Yu T. Durability deterioration of concrete under marine environment from material to structure: a critical review. J Build Eng 2021;35:102074.
[2] Zeng J-J, Feng P, Dai J-G, Zhuge Y. Development and behavior of novel FRP-UHPC tubular members. Eng Struct 2022;266:114540.
[3] Yang JL, Lu SW, Zeng JJ, Wang JZ, Wang ZR. Durability of CFRP-confined seawater sea-sand concrete (SSC) columns under wet-dry cycles in seawater environment. Eng Struct 2023;282:115774.
[4] Dong Z, Wu G, Zhao X-L, Zhu H, Lian J-L. Durability test on the flexural performance of seawater sea-sand concrete beams completely reinforced with FRP bars. Constr Build Mater 2018;192:671–82.
[5] Hao Z-H, Zeng J-J, Chen G-M, Dai J-G, Chen J-F. Durability of FRP-to-concrete bonded joints subjected to 110 months accelerated laboratory and field exposure. Eng Struct 2024;305:117681.
[6] Wei C-C. Conceptual weather environmental forecasting system for identifying potential failure of under-construction structures during typhoons. J Wind Eng Ind Aerodyn 2017;168:48–59.
[7] Ye Y-Y, Smith ST, Zeng J-J, Zhuge Y, Quach W-M. Novel ultra-high-performance concrete composite plates reinforced with FRP grid: Development and mechanical behaviour. Compos Struct 2021;269:114033.
[8] Zeng J-J, Zeng W-B, Ye Y-Y, Liao J, Zhuge Y, Fan T-H. Flexural behavior of FRP grid reinforced ultra-high-performance concrete composite plates with different types of fibers. Eng Struct 2022;272:115020.
[9] Liao J, Zeng J-J, Lin X-C, Zhuge Y, He S-H. Punching shear behavior of FRP grid-reinforced ultra-high performance concrete slabs. J Compos Constr 2023;27:04023031.
[10] Zeng J-J, Ye Y-Y, Liu W-T, Zhuge Y, Liu Y, Yue Q-R. Behaviour of FRP spiral-confined concrete and contribution of FRP longitudinal bars in FRP-RC columns under axial compression. Eng Struct 2023;281:115747.
[11] Zhang D, Yu J, Wu H, Jaworska B, Ellis BR, Li VC. Discontinuous micro-fibers as intrinsic reinforcement for ductile Engineered Cementitious Composites (ECC). Compos Part B 2020;184:107741.
[12] Li H, Xu S, Leung CK. Tensile and flexural properties of ultra high toughness cemontious composite. J Wuhan Univ Technol-Mater Sci Ed 2009;24:677–83.
[13] Yu K, Li L, Yu J, Wang Y, Ye J, Xu Q. Direct tensile properties of engineered cementitious composites: a review. Constr Build Mater 2018;165:346–62.
[14] Ding Y, Yu K-Q, Yu JT, Xu SL. Structural behaviors of ultra-high performance engineered cementitious composites (UHP-ECC) beams subjected to bending-experimental study. Constr Build Mater 2018;177:102–15.
[15] Ranade R, Li VC, Stults MD, Heard WF, Rushing TS. Composite properties of high-strength, high-ductility concrete. Acids Mater J 2013;110:413–22.
[16] Zhu J-X, Weng K-F, Huang B-T, Xu L-Y, Dai J-G. Ultra-high-strength engineered cementitious composites (UHS-ECC) panel reinforced with FRP bar/grid: development and flexural performance. Eng Struct 2024;302:117193.
[17] Huang B-T, Zhu J-X, Weng K-F, Li VC, Dai J-G. Ultra-high-strength engineered/strain-hardening cementitious composites (ECC/SHCC): material design and effect of fiber hybridization. Cem Concr Compos 2022:104464.
[18] Li V, Wang SX. Flexural Behaviors of glass fiber-reinforced polymer (GFRP) reinforced engineered cementitious composite beams. Acids Mater J 2002;99:11–21.
[19] Yan ZT, Zeng JJ, Zhuge Y, Liao JJ, Zhou JK, Ma GW. Compressive behavior of FRP-confined 3D printed ultra-high performance concrete cylinders. J Build Eng 2024;81:108304.
[20] Wang HT, Bian ZN, Chen MS, Hu L, Wu Q. Flexural strengthening of damaged steel beams with prestressed CFRP plates using a novel prestressing system. Eng Struct 2023;284:115953.
[21] Awad ZK, Aravinthan T, Zhuge Y. Experimental and numerical analysis of an innovative GFRP sandwich floor panel under point load. Eng Struct 2012;41:126–35.
[22] Song J, Gao WY, Ouyang JL, Zeng JJ, Yang J, Liu WD. Compressive behavior of heat-damaged square concrete prisms confined with basalt fiber-reinforced polymer jackets. Eng Struct 2021;241:112504.
[23] Lin G, Zeng JJ, Li JX, Chen GM. Chord axial compressive behavior of hybrid FRP-concrete-steel double-skin tubular member T-joints. Thin-Walled Struct 2024;195:111535.
[24] Yan ZW, Bai YL, Ozbakkaloglu T, Gao WY, Zeng JJ. Rate-dependent compressive behavior of concrete confined with large-rupture-strain (LRS) FRP. Compos Struct 2021;272:114199.
[25] Zeng J-J, Liao JJ, Zhuge Y, Guo YC, Zhou JK, Huang ZH, Zhang L. Bond behavior between GFRP bars and seawater sea-sand fiber-reinforced ultra-high strength concrete.Eng. Struct 2022;254:113787.
[26] Zeng J-J, Hao Z-H, Liang Q-J, Zhuge Y, Liu Y. Durability assessment of GFRP bars exposed to combined accelerated aging in alkaline solution and a constant load. Eng Struct 2023;297:116990.
[27] Zeng JJ, Pan BZ, Fan TH, Zhuge Y, Liu F, Li LJ. Shear behavior of FRP-UHPC tubular beams. Compos Struct 2023;307:116576.
[28] Benmokrane B, Wang P, Tan Minh TT, Rahman H, Robert JF. Durability of Glass Fiber-Reinforced Polymer Reinforcing Bars in Concrete Environment. J Compos Constr 2002;6:143–53.
[29] Aguionoiga F., Bradberry T., Trejo D. Time-Dependent Mechanical Property Changes of Glass Fiber-Reinforced Polymers Exposed to High pH Environments. Proc Engineering, Construction, and Operations in Challenging Environments. Texas, United States2004. p. 585–92.
[30] Chen Y, Davalos JF, Ray I, Kim H-Y. Accelerated aging tests for evaluations of durability performance of FRP reinforcing bars for concrete structures. Compos Struct 2007;78:101–11.
[31] Wang Z, Zhao XL, Xian G, Wu G, Singh Raman RK, Al-Saadi S, Haque A. Long-term durability of basalt- and glass-fibre reinforced polymer (BFRP/GFRP) bars in seawater and sea sand concrete environment. Constr Build Mater 2017;139:467–89.
[32] Kamal ASM, Boulfiza M. Durability of GFRP Rebars in Simulated Concrete Solutions under Accelerated Aging Conditions. J Compos Constr 2011;15:473–81.
[33] Dejke V., Tepfers R. Durability and service life prediction of GFRP for concrete reinforcement. Proc 5th Int Conf on Fiber-Reinforced Plastics for Reinforced Concrete Structures (FRPRCS-5). the United Kingdom: Thomas Telford London; 2001. p. 505–16.
[34] Sen R, Mullins G, Salem T. Durability of E-glass/vinylester reinforcement in alkaline solution. Acids Struct J 2002;99:369–75.
[35] Chen Y, Davalos JF, Ray I, Kim HY. Accelerated aging tests for evaluations of durability performance of FRP reinforcing bars for concrete structures. Compos Struct 2007;78:101–11.
[36] Kim H-Y, Park Y-H, You Y-J, Moon C-K. Short-term durability test for GFRP rods under various environmental conditions. Compos Struct 2008;83:37–47.
[37] Sawpan MA, Mamun AA, Holdsworth PG. Long term durability of pultruded polymer composite rebar in concrete environment. Mater Des 2014;57:616–24.
[38] Micelli F, Nanni A. Durability of FRP rods for concrete structures. Constr Build Mater 2004;18:491–503.
[39] Robert M, Benmokrane B. Combined effects of saline solution and moist concrete on long-term durability of GFRP reinforcing bars. Constr Build Mater 2013;38:274–84.
[40] Wang Z, Zhao X-L, Xian G, Wu G, Singh Raman RK, Al-Saadi S. Durability study on interlaminar shear behaviour of basalt-, glass- and carbon-fibre reinforced polymer (B/G/CFRP) bars in seawater sea sand concrete environment. Constr Build Mater 2017;156:985–1004.
[41] Chen Y, Davalos JF, Ray I. Durability prediction for GFRP reinforcing bars using short-term data of accelerated aging tests. J Compos Constr 2006;10:279–86.
[42] Al-Salloum YA, El-Gamal S, Almusallam TH, Alsayed SH, Aqel M. Effect of harsh environmental conditions on the tensile properties of GFRP bars. Compos Part B 2013;45:835–44.
[43] Robert M, Cousin P, Benmokrane B. Durability of GFRP reinforcing bars embedded in moist concrete. J Compos Constr 2009;13:66–73.
[44] Mukherjee A, Arwikar S. Performance of glass fiber-reinforced polymer reinforcing bars in tropical environments-Part I: Structural scale tests. Acids Struct J 2005;102:745.
[45] El-Hassan H, El-Maaddawy T, Al-Sallamin A, Al-Saidy A. Performance evaluation and microstructural characterization of GFRP bars in seawater-contaminated concrete. Constr Build Mater 2017;147:66–78.
[46] Wang J, GangaRao H, Liang R, Zhou D, Liu W, Fang Y. Durability of glass fiber-reinforced polymer composites under the combined effects of moisture and sustained loads. J Reinf Plast Compos 2015;34:1739–54.
[47] Wang Z, Zhao X-L, Xian G, Wu G, Raman RKS, Al-Saadi S. Effect of sustained load and seawater and sea sand concrete environment on durability of basalt- and glass-fibre reinforced polymer (B/GFRP) bars. Corros Sci 2018;138:200–18.
[48] Nkurunziza G, Benmokrane B, Debaiky AS, Masmoudi R. Effect of sustained load and environment on long-term tensile properties of glass fiber-reinforced polymer reinforcing bars. Acids Struct J 2005;102:615–21.
[49] JSCE (Japan Society of Civil Engineers). Recommendations for Design and Construction of High Performance Fiber Reinforced Cement Composites with Multiple Fine Cracks (HPFRCC). Japan: Concrete Engineering Series 82; 2008.
[50] Benmokrane B, Elgabbas F, Ahmed EA, Cousin P. Characterization and comparative durability study of glass/vinylester, basalt/vinylester, and basalt/epoxy FRP bars. J Compos Constr 2015;19.
[51] CSA (Canadian Standards Association). Design and construction of building components with fibre-reinforced polymers. Canada: CSA-S806; 2012.
[52] McCombe G, Rouse J, Trask R, Withers P, Bond I. X-ray damage characterisation in self-healing fibre reinforced polymers. Compos, Part A 2012;43:613–20.
[53] Nagura A, Okamoto K, Itoh K, Imai Y, Shimamoto D, Hotta Y. The Ni-plated carbon fiber as a tracer for observation of the fiber orientation in the carbon fiber reinforced plastic with X-ray CT. Compos Part B 2015;76:38–43.
[54] Yoshimura A, Hosoya R, Koyanagi J, Ogasawara T. X-ray computed tomography used to measure fiber orientation in CFRP laminates. Adv Compos Mater 2016;25:19–30.
[55] Zeng J-J, Hao Z-H, Liang X-C, Li J-L, Zhuge Y, Liu F, Li L-J. Durability assessment of hybrid double-skin tubular columns (DSTCs) under simulated marine environments. Eng Struct 2024;301:117168.
[56] Wu G, Dong ZQ, Wang X, Zhu Y, Wu ZS. Prediction of long-term performance and durability of BFRP bars under the combined effect of sustained load and corrosive solutions. J Compos Constr 2015;19:04014058.
[57] Zhou J-K, Hao Z-H, Zeng J-J, Feng S-Z, Liang Q-J, Zhao B, Feng R, Zhuge Y. Durability assessment of GFRP bars embedded in UHP-ECCs subjected to an accelerated aging environment with sustained loading. Constr Build Mater 2024;419:135364.